Additive manufacturing of metallic materials – a review

Yi Zhang[1], Linmin Wu[1], Xingye Guo[1], Stephen Kane, Yifan Deng[2], Yeon-Gil Jung[3], Je-Hyun Lee[3], Jing Zhang[1*]
1. Indiana University – Purdue University Indianapolis, Indianapolis, IN 46202, USA
2. University of California at San Diego, La Jolla, CA 92093, USA
3. Changwon National University, Changwon, Gyeongnam 641-773, Republic of Korea

*Corresponding author: jz29@iupui.edu

Abstract

In this review article the latest developments of the four most common additive manufacturing methods for metallic materials are reviewed, including powder bed fusion, direct energy deposition, binder jetting and sheet lamination. In addition to the process principles, the microstructures and mechanical properties of AM fabricated parts are comprehensively compared and evaluated. Finally, several future research directions are suggested.

Keywords: Additive manufacturing; metal; process; microstructure; mechanical property.

Zhang, Y., Wu, L., Guo, X., Kane, S., Deng, Y., Jung, Y.-G., … Zhang, J. (2017). Additive Manufacturing of Metallic Materials: A Review. Journal of Materials Engineering and Performance, 1–13. https://doi.org/10.1007/s11665-017-2747-y

1. Introduction

In the 1980s, rapid prototyping (RP) was first introduced to produce a 3D prototype layer-by-layer from a computer-aided-design (CAD)[1]. With the advancement of RP technique and the need of high-efficiency manufacturing with the ability to produce complex parts, the first additive manufacturing (AM) technique was brought on stage by researchers at University of Texas Austin in 1986. In the past 30 years, many new AM processes have been developed. These processes show several significant advantages, including versatile geometric capability, minimum human interaction requirement, and reduced design cycle time [2]. Since then, AM has been successfully applied in numerous fields. Functional AM parts with complex geometries have been used as aircraft engine components [3, 4], automobile parts [5], and space components [6] [7]. According to the ASTM standard published in 2009 [8], the AM techniques can be classified into the following categories, as listed in Table 1.

Table 1: Summary of AM processes classified by ASTM F42 [9] and their typical applications

Process	Application
Material extrusion	Plastic prototyping
Vat polymerization	Prototyping, high surface finish parts
Binder jetting	Prototyping, investment casting
Material jetting	Visual prototyping
Powder bed fusion	Functional prototyping, engineering functional parts
Sheet lamination	Prototyping
Direct energy deposition	Prototyping, functional parts, repairing metal parts and fixtures

AM processes of metallic materials generally include (i) powder bed fusion (PBF), (ii) direct energy deposition (DED), (iii) binder jetting (BJ), and (iv) sheet lamination (SL). Vat polymerization is only capable of fabricating polymer materials. Other processes have been experimentally tested for metal fabrication, e.g., liquid metal extrusion [10] and material jetting [11, 12]. However, they are still in early stages of development, and there are no commercial systems yet.

The currently available commercial metal AM systems with their manufacturers are listed in Table 2. The systems are classified based on the ASTM standard. The processing information, including layer thickness range and laser beam diameter, along with system energy sources, is also listed.

Laser based powder bed fusion, including selective laser melting (SLM), selective laser sintering (SLS), direct metal laser sintering (DMLS), are the most popular AM processes. In these processes, laser power is usually in the range of 100-1000 W depending on the manufacturer. The thickness of each build layer of laser based PBF can be as small as 20 μm, which shows the advantage in terms of resolution over other AM processes. Arcam is the manufacturer for electron beam based PBF. The power of an e-beam is much higher than a laser source, and a thicker layer of metallic powder can be built in each scan. Trumpf provides both powder feed DED and laser based PBF. ExOne and Fabrisonic are the manufacturers for BJ and SL systems that are suitable for AM fabrication of metallic materials.

Table 2: Commercial AM systems for metallic materials

Manufacturer	System	Process	Layer thickness (μm)	Laser focus diameter (μm)	Energy source
Concept laser [13]	M1 cusing	PBF(SLM)	20-80	50	Fibre laser 200 W - 400 W
Sisma [14]	MYSINT300	PBF(SLM)	20-50	100-500	Fibre laser 500 W
SLM Solutions [15]	SLM500	PBF(SLM)	20-74	80-115	Quad fibre lasers 4 x 700 W
Realizer [16]	SLM300i	PBF(SLM)	20-100	N/A	Fibre laser 400 W - 1000 W
Farsoon [17]	FS271M	PBF(SLS)	20-80	40-100	Yb-fibre laser, 200 W
EOS [18]	M 400	PBF(DMLS)	N/A	90	Yb-fibre laser, 1000 W
Arcam AB [19]	Arcam Q20plus	PBF(EBM)	140	--	Electron beam 3000 W
Optomec [20]	LENS Print Engine	DED(LENS)	25	--	IPG Fiber Laser 1 - 2 kW
Sciaky [21]	EBAM 300	DED (wire feed)	N/A	--	Electron beam
Trumpf [22]	TruLaser Cell Series 7000	DED (powder feed)	N/A	--	CO2 laser (15000 W) or YAG laser (6600 W)
ExOne [23]	M print	BJ	150	--	--
Fabrisonic [24]	SonicLayer 7200	SL(UAM)	150	--	20 kHz ultrasonic vibration sonotrode

Kaufui *et al.* conducted a review in 2012 on the development and application of rapid prototyping [25]. In the review, two aspects limiting the application of AM from industrial applications were discussed, these being material capability and parts accuracy. Another review on the microstructures of laser/electron beam based rapid prototypes was conducted by Murr in 2012 [26]. The review paper discussed how the material microstructure architectures can be controlled by AM processes. In 2014, Tapia *et al.* reviewed the process monitoring and control of metal AM systems [27]. The rationale and importance of research on real-time control of AM were identified, in terms of improving the product accuracy and material/time efficiency. Also in 2014, Frazier discussed AM processes, material properties, and business considerations [28]. The AM processed metallic materials were analyzed in terms of their microstructure evolution and static/dynamic properties. The paper discussed the mechanical properties of AM parts to show the process-microstructure-properties relationship, which was further discussed by other researchers [29-31]. In 2016, Lewandowski compared the tensile properties and fatigue crack behaviors of Ti6Al4V fabricated through PBF and DED based AM processes [32]. The results showed that the mechanical properties may vary with AM process and AM machine. Additional review articles include the material properties and qualifications, as well as the economic or environmental impacts of AM processes [33, 34].

The objective of this review article is two-fold. The first is to provide the latest information regarding the AM metallic material microstructures and mechanical properties. The second is to cover the process-microstructure-property correlation of binder jetting, sheet lamination, powder bed diffusion and direct energy deposition processes, thus providing a comprehensive review of all major AM processes for metallic materials. The structure of this review article is arranged into four major sections from section 2 to section 5, based on the four major AM processes. Each section is further divided into sub-sections of process description, typical microstructures, and a compilation of mechanical properties. Section 6 provides the conclusion and suggested future research directions.

2. Powder bed fusion

Powder bed fusion (PBF) uses a high-energy power source to selectively melt or sinter a metallic powder bed. Depending on the type of power source, PBF can be further divided into two major techniques: selective laser melting (SLM) which uses a high-intensity laser, and electron beam melting (EBM), which uses an electron beam. Both processes need a building platform to hold the powder.

2.1 Powder bed fusion equipment and process

Even though the principles of these two processes are similar, the processing steps are quite different. The schematics of the SLM set up are shown in Figure 1(a)[35]. In the SLM process, the laser beam passes through a system of lenses and reflected by a mirror onto the platform surface. The mirrors are used to control the laser beam spot movement on the planar (X and Y) directions on the designed paths. After a layer of powder is selectively melted, the platform moves downward, a recoating blade or brush pushes another layer of fresh powder from the powder tank to the top of the previously built surface, and the laser scan process repeats. The building chamber of an SLM machine is filled with an inert gas, argon in most cases, to avoid oxidization of metallic powders at high temperatures.

The EBM process is essentially developed from the scanning electron microscope (SEM) technique [29]. It utilizes a much higher power electron beam to selectively melt the powder. Vacuum condition is required for the EBM process. As shown in Figure 1(b)[36], the electron beam source is located on the top of the powder bed. The movement of the electron beam is directly controlled by a lens system. A powder hopper pours fresh powder onto the side of the platform, and then a layer of powder is coated by a rake on the top of previously melted layer.

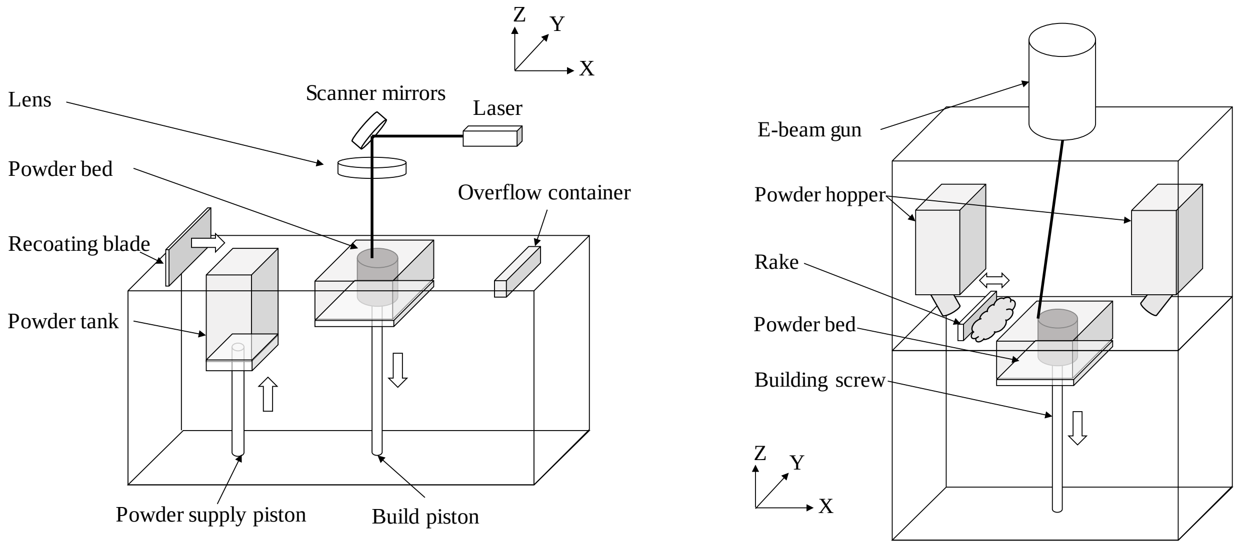

(a) (b)

Figure 1: Schematics of powder bed fusion equipment. (a) Selective laser melting, and (b) electron beam melting.

2.2 Microstructures and mechanical properties of powder bed fusion fabricated parts

Several studies have been focused on relating the PBF process parameters to the resulting microstructure [35, 37]. Although at high processing temperatures, most of the scanned powder is melted and densified, the PBF fabricated parts still contain some porosities [36]. Figure 2 shows the microstructure of an SLM processed Ti-6Al-4V part [38]. From the top view (Figure 2a), one can easily observe the parallelly orientated grains with /// or \\\ band-shaped patterns. Each of these patterns has a width of the scan hatch space and it follows the laser scan direction. The highly orientated grains are created by a high temperature gradient during fast heating and cooling process. From the side view (Figure 2b), the grains are mostly vertical with elongated shapes. The vertically columnar grains are tilted according to the scan direction. Horizontally dark bands can be observed due to the layer-wise AM process. Two types of pore can be found in the PBF parts: the pores due to trapped gas in the powder bed (Figure 2c), and the pores caused by insufficient melting (Figure 2d), which are mostly seen near the edge regions [39].

The grain microstructures of PBF parts are mostly affected by two factors: the temperature gradient and the solidification interface velocity. Columnar grains develop when the temperature gradient is large and the interface velocity is small. In contrast, small temperature gradient and large interface velocity will form equiaxed grains. This grain transformation can be calculated by the dendrite growth model by Hunt in 1984 [40]. Based on this model, Nastac *et al*. investigated several nickel alloys, and generated the solidification maps for Inconel 718 and RS5 alloys [41]. Sames *et al.* developed a processing window for the EBM process. Their works show that Arcam fabricated Inconel 718 grain growth can be specifically controlled by these two factors [42].

Both temperature gradient and interface velocity can be affected by processing parameters like scan speed and laser / e-beam power. Using process design to control the microstructure has been mentioned in many recent works. Dehoff *et al.* developed an EBM processing strategy that was able to produce fine grained Inconel 718 [43]. Later, Helmer *et al.* studied the processing window, and they also obtained fine epitaxial grains from columnar grains [44].

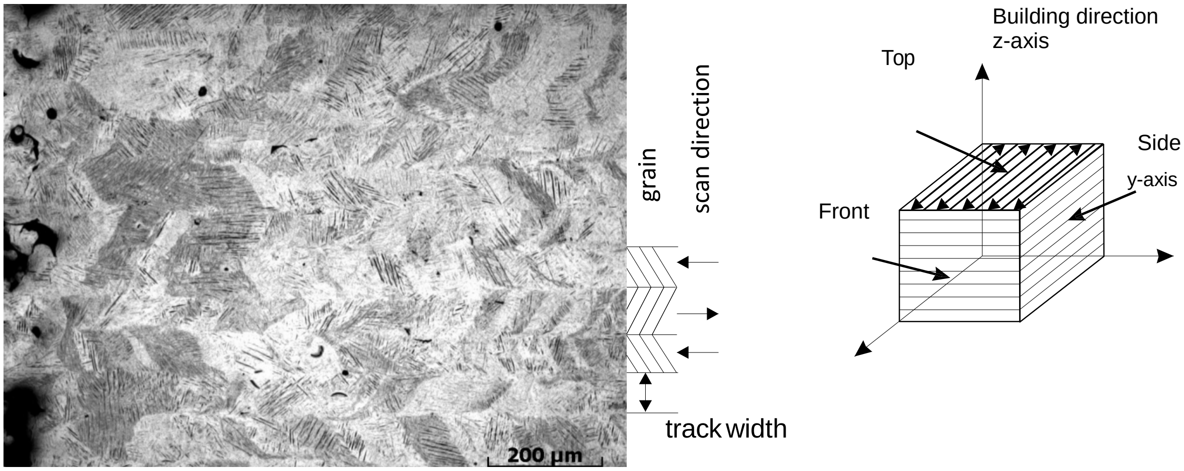
grain
scan direction
track width
200 µm
Building direction
z-axis
Top
Side
y-axis
Front

(a)

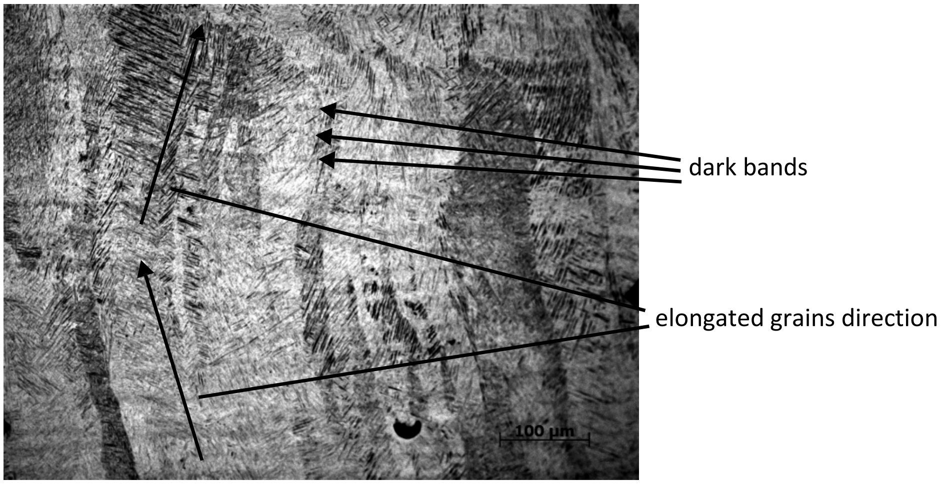
dark bands
elongated grains direction
100 µm

(b)

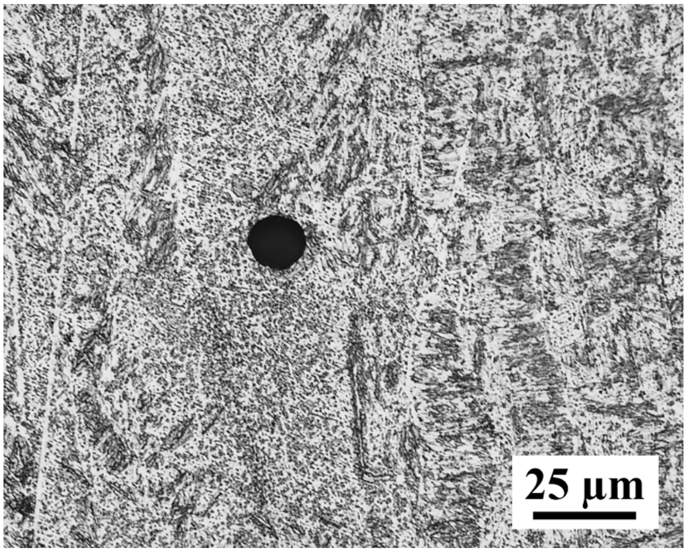
25 µm

(c)

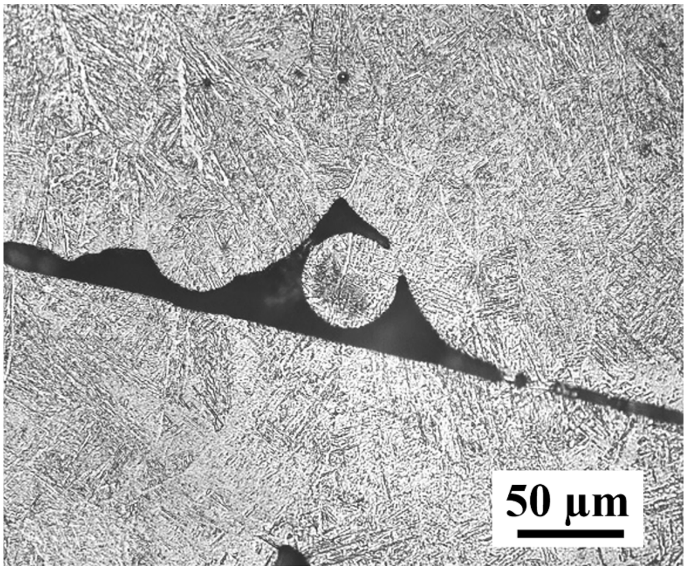

(d)

Figure 2: (a) Microstructures of the SLM built Ti-6Al-4V parts with top (a) and side (b) views [38], (c) pore due to trapped gas, and (d) pore due to insufficient heating [39].

The mechanical properties of both SLM and EBM processed materials are crucial to their applications. Important mechanical properties such as elastic modulus, ductility, and fatigue of PBF parts were reported [30, 45-49]. Kruth *et al.* presented the binding mechanisms that affect the mechanical properties of AM parts [50]. The binding mechanisms can be divided into four categories based on the degree of melting: (1) solid state sintering, (2) chemically induced binding, (3) partial melting, and (4) full melting[50]. PBF parts show anisotropic properties including elastic modulus, yield stress and ultimate stress[47]. This anisotropy is mainly caused by insufficient heat energy which induces a lack of fusion at the interface between each layer, so that the building direction is weaker than the scanned planar direction.

For both PBF and DED processes, the properties of Ti6Al4V alloy have been extensively investigated. This is due to the high demand of this material for aerospace and medical implant applications. Also, as suggested by Yang *et al*, Ti6Al4V is difficult to fabricate using conventional manufacturing methods [51]. This problem can be easily solved by AM, since only powder will be used. The tensile properties of PBF fabricated Ti6Al4V parts were tested by many researchers, and the resulting data are listed in Table 3. The mechanical properties, including Young’s modulus, yield strength, ultimate strength and strain at failure are compared to the traditional wrought Ti6Al4V. It should be noted that the orientation in Table 3 shows the tensile direction, where horizontal refers the in-plane direction of each deposited layer, and vertical refers the direction of accumulation.

Table 3: Mechanical properties of metallic materials fabricated by powder bed fusion technologies

Process	Equipment	Condition	Orientation	Young's modulus (GPa)	Yield strength (MPa)	Ultimate strength (MPa)	Failure strain
Wrought [52]	N/A	As fabricated	Longitudinal	113	945	979	0.100
SLM	EOSINT M270 [52]	As fabricated	Horizontal	109	972	1034	0.055
			Vertical	115	1096	1130	0.012
		HIP	Hor. & vert.	112	862	931	0.240
	Concept Laser M2 [53]	As fabricated	Horizontal	105	1070	1250	0.060
			Vertical	102	1050	1180	0.080
		HIP	Horizontal	112	1000	1060	0.125
			Vertical	110	920	1000	0.160
	Realizer (SLM300i) [54]	As fabricated	Vertical	119	967	117	0.089
	Trumpf (LF250) [55]	As fabricated	Horizontal	105	1137	1206	0.076
			Vertical	102	962	1166	0.017
		Heat treated	Horizontal	103	944	1036	0.085
			Vertical	98	925	1040	0.075
EBM	Arcam A2 [56]	As fabricated	Horizontal	NA	1006	1066	0.150
			Vertical	NA	1001	1073	0.108
	Arcam S12 [57]	As fabricated	Horizontal	NA	983	1030	0.122
			Vertical	NA	984	1033	0.090
	Arcam S400 [58]	As fabricated	Horizontal	104	844	917	0.088
			Vertical	101	782	842	0.099
		machined	Horizontal	114	899	978	0.095
			Vertical	115	869	928	0.099
	Arcam [59]	As fabricated	N/A	118	830	915	0.131
		HIP	N/A	117	795	870	0.137

As shown in the table, the Young's moduli of both SLM and EBM processed parts show similar values to the wrought one. Approximately a 10% difference can be observed when comparing the horizontal and vertical orientations. For the SLM processed parts, the yield and ultimate strengths are even better than that of the conventional wrought material. This is mainly because PBF uses very fine powders as raw material. The as-fabricated parts behave more brittle with very limited failure strains. Effective post treatment, for example, hot isostatic pressing (HIP) doubles the elongation, but HIP process decreases the yield and ultimate strengths. The EBM processed parts show that the vertical orientation has 30% less elongation than the horizontal orientation, but no obvious difference is found in the yield and ultimate strengths. A machining treatment for the EBM parts can increase the Young's modulus, yield strength and ultimate strength, but the elongation at failure is not changed.

The mechanical properties of other materials, including aluminum alloys and stainless steels, were also studied. However, the available data are not as abundant as for Ti6Al4V. The effect of heat treatment on the tensile properties of AlSi10Mg was studied by Krishnan [60]. Tensile properties of 15-5 stainless steel and fatigue properties of 316L were presented in Ref [61] and Ref [62], respectively.

It is noted that PBF processed parts are prone to several issues, due to the weak bonding between layers and the complicated thermal history. High temperature gradients cause thermal residual stress that accumulates as the layers are built up, resulting in distortion and wrapping of the product. Layer delamination and cracking are also common due to thermal stress and the weak bonding between layers.

3. Direct energy deposition

3.1 Direct energy deposition equipment and process

Another well-developed manufacturing technique is direct energy deposition (DED). Instead of using a powder bed, DED process uses injected metal powder flow or metal wire as feedstocks, along with an energy source such as laser or electron beam, to melt and deposit the material on the top of a substrate. DED techniques can be divided into two major categories based on the feedstocks. The first category includes methods developed from traditional welding technique using metal wire as a feedstock. The second method named Laser Engineered Net Shaping (LENS)[63] was developed by Sandia National Laboratory in 1996, which uses powder flow as a feedstock.

The schematic of a LENS machine is shown in Figure 3. In a building chamber, a Nd: YAG laser beam focuses on a point on the building platform using a lens system, and at the same time, metal powder is injected to the point through a powder nozzle. The powder flows into the melt pool at the same time as the laser source or the building platform moves. The melted powder and the materials beneath solidify quickly, thus forming a layer of material. After one layer is built, the laser lenses and powder nozzle move up, and the laser heating and powder injection processes repeat for the next layer[63].

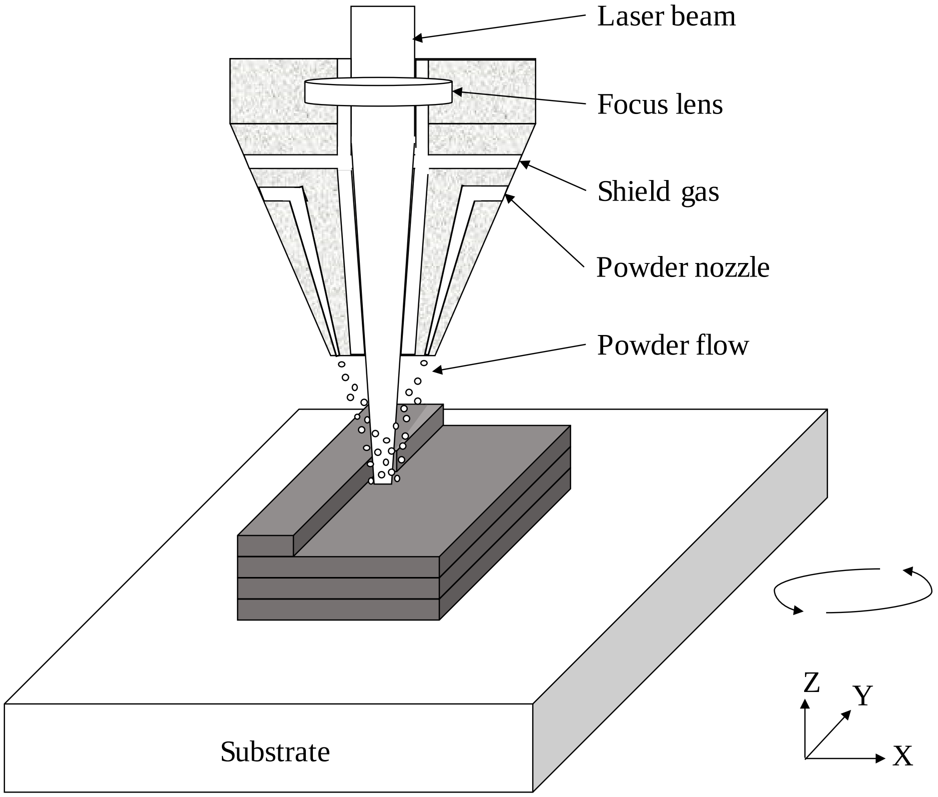

Figure 3: Schematic of LENS process.

Electron beam is another power source for the DED system due to its high energy density. By using an electron beam, high accuracy and good surface finishing can be achieved with low deposition rates. The Electron Beam Freeform Fabrication (EBF^3) process was developed by NASA [64]. It is primarily used for space-based applications. The EBF^3 process uses a metal wire filament instead of powder injection. With electron beam or laser source, the front end of the metal wire is melted and selectively sprayed on the top of a substrate to form a material layer.

3.2 Microstructures and mechanical properties of direct energy deposition fabricated parts

A comprehensive study on the microstructure of LENS fabricated parts was first reported by Griffith *et al.* [65, 66]. In their study, the tensile properties of wrought materials were used as a reference for comparison. They found that the yield strength of LENS fabricated parts is very similar to wrought parts, and the tensile properties of LENS fabricated parts could be optimized by adjusting processing parameters. Later several work done by Wu *et al.* [67-69] showed that the morphologies and size of the typical columnar grains and lamellar microstructures are mainly affected by laser power and laser scan speed. Wang *et al.* [70] identified two solidification mechanisms in the local melt pool. They suggested a strategy that uses mass flow rate to control the grain structures. High mass flow rate leads to near-full equiaxed grains, and low mass flow rate leads to full columnar grains.

The microstructure evolution of DED process can be extracted from the grain morphology. There are two typical solidification mechanisms: (1) heterogeneous nucleation on partially melted powders for equiaxed grains, and (2) epitaxial growth from the melt pool bottom for columnar grains. These two mechanisms compete with each other during deposition, therefore the microstructures of the product can vary. Along the deposition track, the grains show a layered microstructure as seen in the heat affected zone (HAZ) in Figure 4[70]. Equiaxed grains form on the top region where laser is applied. The depth of this layer is marked as d_{EG} in the figure. The next region shows a layer of columnar grain structure, where d_{PM} denotes the penetration depth. The layered grain distribution can be seen from both the transverse direction (Figure 4 (a)) and longitudinal direction (Figure 4 (b)).

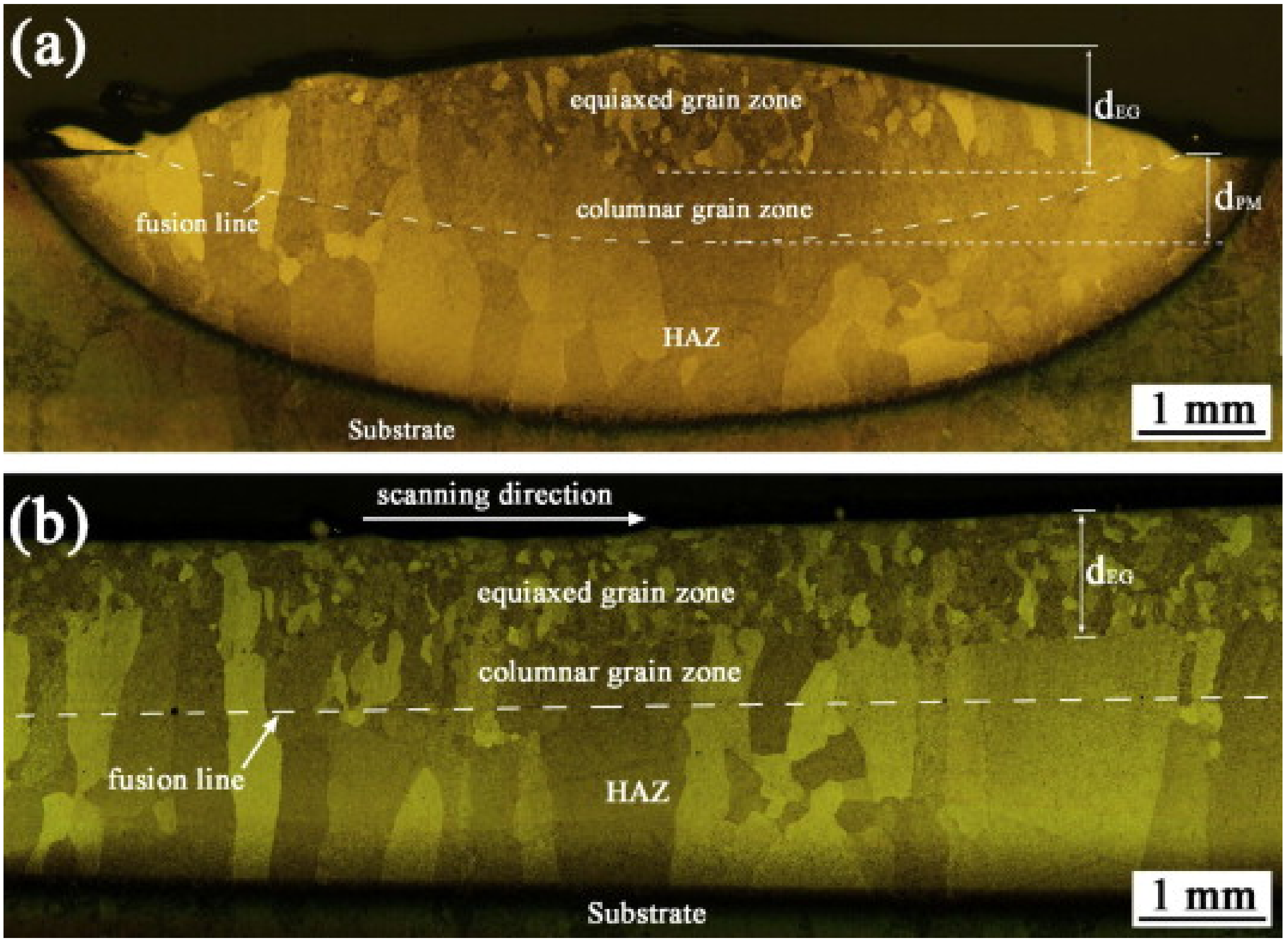

Figure 4: Microstructures of grains in the heat affected zone during DED process: (a) transverse direction, and (b) longitudinal direction [70].

The mechanical properties of LENS fabricated alloy, Ti6Al4V, and EBF^3 fabricated nickel alloy (Inconel 718) are summarized in Table 4. The powder fed LENS and direct laser deposition (DLD) show the similar results as PBF parts. The Young's modulus is very close to the wrought, and very small failure strains are observed in the as-fabricated samples. With the HIP treatment, the failure strain can be improved at least two-folds, but the yield and ultimate strengths decrease when HIP is applied. The changes in strength are due to the fact that HIP'ed materials have a lower alphaplatelet thickness. The difference in ductility is probably due to the presence of porosity in the as-fabricated material. It is noted that for yield strength, ultimate strength and failure strain, the difference between the horizontal and vertical directions is larger than that of PBF products, which means that the mechanical properties of the powder fed DED (LENS) fabricated parts show even higher anisotropy than the PBF parts. Since in DED, the layer thickness is usually greater than that of PBF, therefore less fusion occurs at the layer interfaces [70-72]. For the wire fed DED process (EBF^3), the tensile properties of two planar orientations (parallel and perpendicular to the wire) were compared. The results show that heat treatment can fill the gaps or voids between adjacent wires, therefore enhancing the mechanical properties. However, other in-plane orientations will not be affected.

316L stainless steel shows a similar trend as Ti6Al4V, where ~16% ultimate strength difference and 53% elongation difference were found. Other mechanical properties including hardness and surface roughness also show a difference at different printing orientations. For example, the microhardness difference of austenite printed at 0^o (samples printed horizontally) and 90^o (samples printed vertically) is more than 25% [70].

Table 4: Mechanical properties of Ti6Al4V and Inconel 718 fabricated by direct energy deposition

Feedstock	Process	Material	Condition	Orientation	Young's modulus (GPa)	Yield strength (MPa)	Ultimate strength (MPa)	Failure strain
Powder fed	Wrought [52]	Ti6Al4V	As fabricated	Longitudinal	113	945	979	0.100
	Optomec LENS [71]	Ti6Al4V	As fabricated	Horizontal	116	1066	1111	0.053
				Vertical	112	832	832	0.008
			HIP	Horizontal	118	949	1006	0.131
				Vertical	114	899	1002	0.118
	Optomec LENS [73]		As fabricated	Vertical	119	908	1038	0.038
			Heat treated	Vertical	118	957	1097	0.034
			Annealed	Vertical	112	959	1049	0.037
	Trumpf DLD [74]		As fabricated	Horizontal	NA	950	1025	0.12
				Vertical	NA	950	1025	0.05
			HIP	Hor. &Vert.	NA	850	920	0.17
Wire fed	Wrought [75]	Inconel 718	As fabricated	Longitudinal	202	1195	1372	N/A
	EBF^3 [76]	Inconel 718	As fabricated	Hor. (parallel to wire)	138	655	978	N/A
				Hor. (perpendicular to wire)	194	699	936	N/A
			Heat treated	Hor. (parallel to wire)	174	986	1114	N/A
				Hor. (perpendicular to wire)	192	998	1162	N/A

Since the PBF and DED undergo similar processes with a high temperature gradient, the issues of thermal residual stress and distortion also exist in the DED process. Different from the PBF systems, some advanced DED machines use a 5- or more axis system instead of 3-axis, which enable the fabrication of larger parts with an optimal manufacturing process. Also, different from PBF process, where vacuum or inert gas must be applied, in the DED process, for non-reactive metals, an inert gas environment is not necessary. To protect the material from oxidization, a shielding gas flow is applied to the melt pool area.

4. Binder jetting

4.1 Binder jetting equipment and process

Binder jetting sometimes is named as powder bed and inkjet head 3D printing. It was first developed and patented by Saches *et al.* in 1993[77]. The idea is to extend the normal two-dimensional printing to the third dimension. In practice, it uses one or more nozzles to inject liquid binder on the top of a powder bed, gluing the powder together. The nozzles move according to the designed path until a thin layer of powder is bonded. Finally, a three-dimensional object is formed by stacking of layers.

A schematic of binder jetting equipment is shown in Figure 5. The system consists of a building platform and a powder tank. Before the binder jetting process starts, a thin layer of powder is distributed on the platform by a leveling roller. Then, the inkjet nozzle moves along the X and Y-directions to locally distribute and adhere powder together. After each layer of powder is bonded, the platform moves down (Z direction) for a small distance, another layer of powder is distributed, and the binder injection process repeats. When all the layers are built, the glued object, which is also called the "green body", is taken from the powder bed for further post processing.

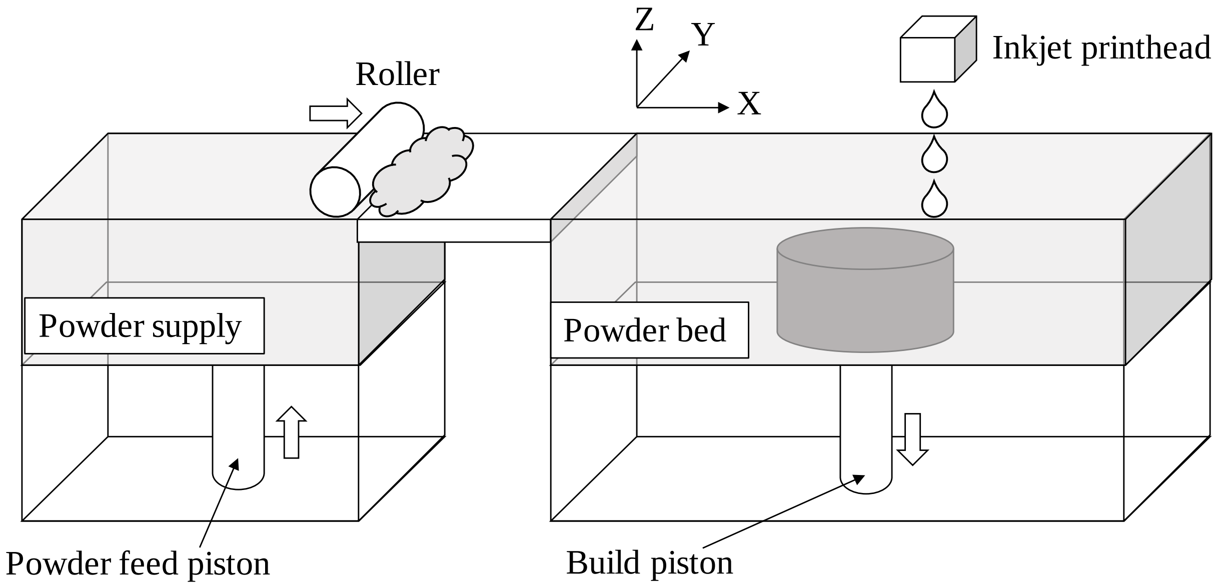

Figure 5: Schematic of binder jetting 3D printing technology.

Post processing of binder jetted objects is often more complicated than other AM techniques, especially for metallic materials. To produce a solid metallic part that has desirable mechanical strength, the "green body" needs to be cured for approximately 6-12 hours and then heat treated above 1000 ^{o}C for 24-36 hours. The heat treatment involves sintering, consolidation and sometimes infiltration, and burning of the binder. The loosely packed metallic powder is bonded together through powder sintering and densification, so that the overall density and strength of the part can be increased. In some cases, metals with a low melting point, e.g., bronze, can be used to infiltrate other higher-melting temperature metals. By doing this, the ductility of the binder jetting product can be increased [78].

4.2 Microstructures and mechanical properties of binder jetting fabricated parts

For metallic materials, post processing is a crucial step, since it can directly affect the part's geometry and density. Powder size, layer thickness, and heat treatment conditions are the major processing parameters that control the part's density. Finer powder often increases the density of the product. However, the efficiency of densification is decreased due to the powder spreading issue [79]. Larger layer thickness reduces the processing time but increases the porosity.

Different heat treatment methods, including sintering, solutionizing, and aging, affect the microstructures and mechanical properties. Mostafaei *et al.* [80, 81] conducted studies showing that, among many heat treatment methods, properly aged parts resulted in higher tensile strength, elongation, and hardness.

Recently, reactive sintering was introduced to the binder jetting post process, which gives the opportunity to modify the chemical composition of the product during the fabrication process. For example, Dilip *et al.* showed the feasibility of fabricating TiAl by using Ti6Al4V and Al powders [82]. The scanning electron microscope (SEM) images of binder jetted nickel alloy 625 under different heat treatment conditions are shown in Figure 6(a)-(c). Near fully dense structures can be achieved by each type of the treatment; however, different heat treatments introduce varying alloy phases which affect the mechanical properties. The solutionized and aged samples show higher hardness and toughness than the sintered samples, which is attributed to the carbide precipitates dissolved by the solution and formed intermetallic precipitates during the aging process. The comparisons of microhardness and stress-strain curves in different heat treated samples are shown in Figure 6 (d) and Figure 6 (e).

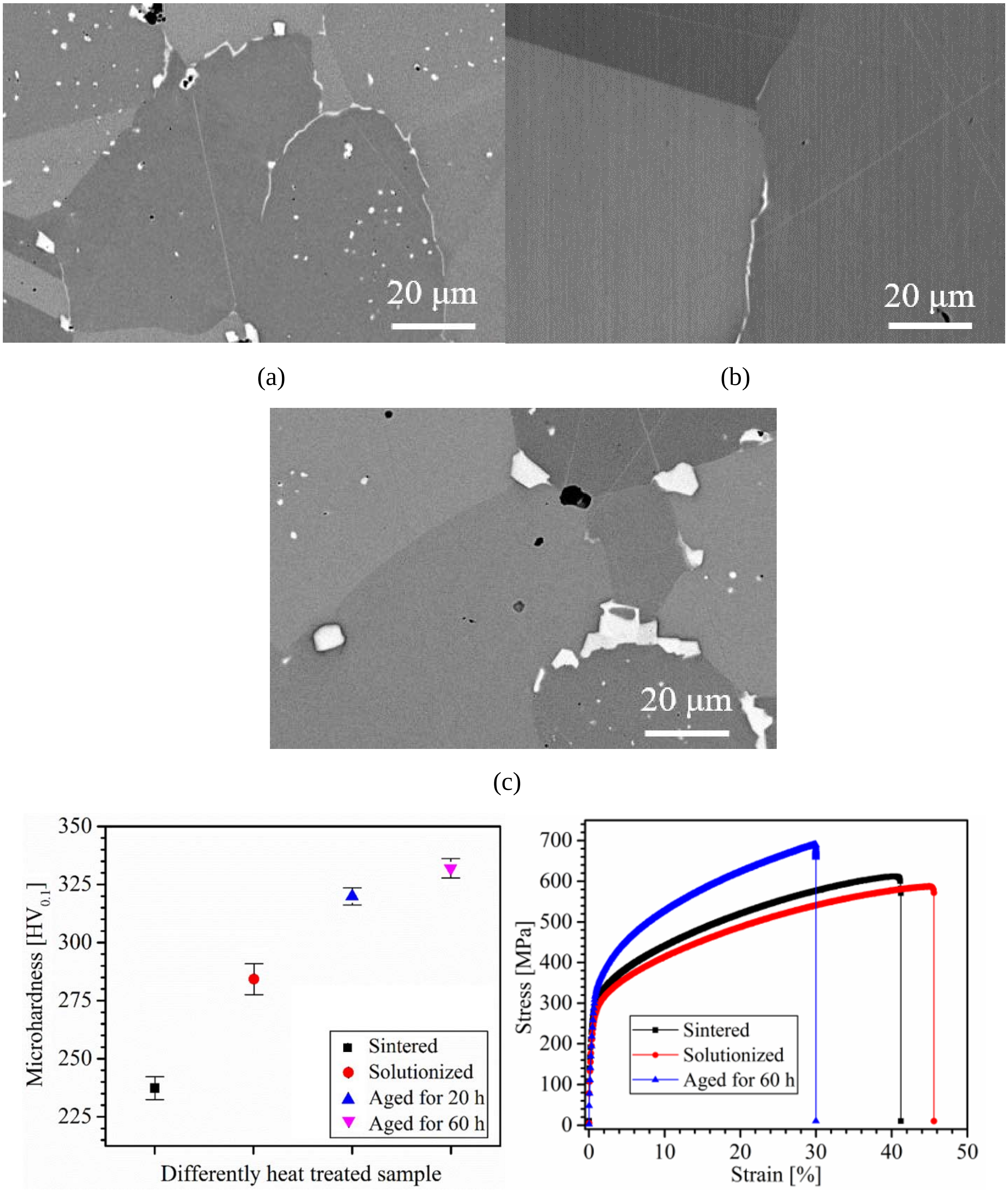

(a) (b)

(c)

(d) (e)

Figure 6: Microstructures of (a) the sintered, (b) solutionized, (c) aged samples; and mechanical properties as illustrated in (d) microhardness values, (e) stress-strain curves [80].

A unique feature of binder jetted metallic materials is that, even though the “green bodies” are the same, the mechanical properties of binder jetted metals and alloys can vary significantly. Table 5 shows the fabricated products after heat treatment (sintering). The relative density varies from 60% to near fully dense (>97%). With the same material of bronze, the ultimate strengths vary from 8 to 117 MPa. For Inconel 625, as the sintering temperature increases, the hardness and ultimate strength decrease. One should note that all the Inconel 625 samples are almost fully dense, therefore the trend observed from bronze does not apply anymore. The decrease of Inconel’s mechanical properties is attributed to 1) grain coarsing, 2) element segregation at grain boundary, 3) laves phases formation due to Nb and Mo concentration at the grain boundary, and 4) NbC from the material matrix [83].

Table 5: Mechanical properties and relative densities of metallic parts with varying sintering temperatures

Equipment	Material	Sintering temperature (°C)	Relative density (%)	Ultimate strength (MPa)	Failure strain	Hardness
ExOne Ex-Lab [84]	Fe-Mn alloy	1200	60.7	228	0.014	N/A
ExOne R2 3D [85]	Bronze	1040	N/A	8	N/A	N/A
		1060	78.2	73	N/A	N/A
		1080	85.5	117	N/A	N/A
ExOne M-Flex [83]	Inconel 625	1280	99.6	612	0.41	237 (HV)
		1290	98	588	0.45	195 (HV)
		1300	97.9	522	0.356	185 (HV)

The printing process of a binder jetting system is usually faster than other AM methods, since it operates at lower temperatures and multiple nozzles can print simultaneously. In some advanced binder jetting systems, only a few seconds are required for printing each layer [86]. However, with the consideration of time-consuming post process, the overall fabrication speed of binder jetting is slower than other AM techniques. Moreover, part shrinkage cannot be avoided during the post sintering process [79, 87]. More research is needed to improve the geometric accuracy of the finished part.

5. Sheet lamination

5.1 Sheet lamination equipment and process

The sheet lamination or laminated object manufacturing (LOM) is a manufacturing technique that uses metallic sheets as feedstock. It uses a localized energy source, usually ultrasonic or laser, to bond a stack of precision cut metal sheets to form a 3-D object [88]. The most commonly used manufacturing technique is ultrasonic additive manufacturing (UAM) or ultrasonic consolidation (UC), which was first introduced and patented by White [89, 90]. By applying ultrasonic wave and mechanical pressure on sheet metal stacks at room temperature, the interfaces of stacked sheets are bonded by diffusion rather than melting. The stacked sheets are bonded layer-by-layer to form a 3D object without using any heat source. Before ultrasonic consolidation bonding, the metallic sheets are often cut according to the designed geometry. Traditional polishing is optionally applied during or after the consolidation process to achieve a detailed finishing.

The working process of a UAM equipment is illustrated in Figure 7. Metallic sheets are laid out and stacked on a base plate. A digitally controlled sonotrode moves along the rolling direction to provide ultrasonic vibration and pressure. A new metallic sheet is therefore bonded with the previously built parts, due to the high-frequency vibration of the sonotrode. During this process, the temperature of the consolidated region increases due to frictional heat at the bonded interfaces. In order to avoid thermal residual stress, there is a short period of cooling between the manufacturing of each layer. After building all of the layers, the product is cut from the base plate and then polished for better surface finishing.

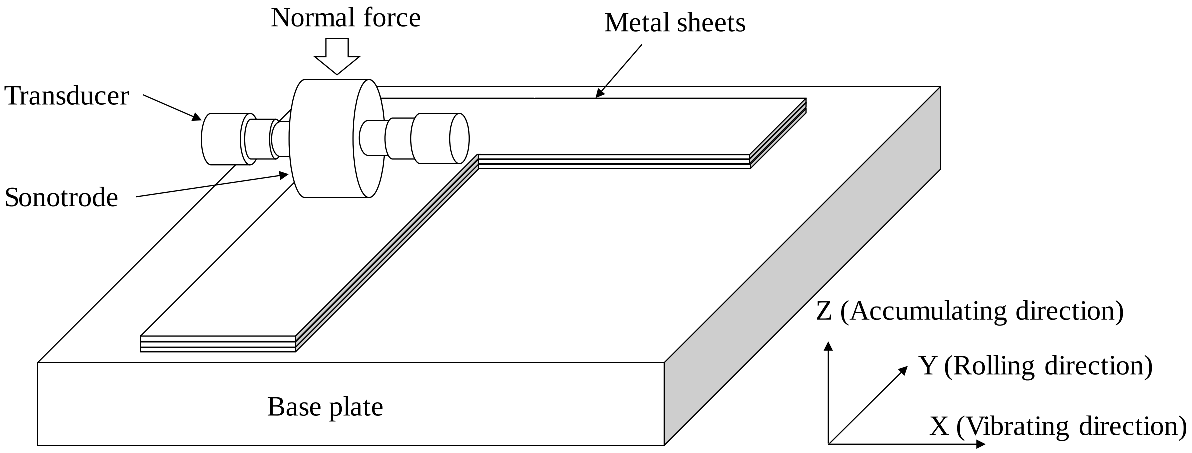

Figure 7: Schematic of the UAM process.

5.2 Microstructures and mechanical properties of sheet lamination fabricated parts

The bonding mechanisms in the sheet lamination process were recently studied by examining the microstructures of bonded interfaces [91]. A schematic of microstructure evolution during the sheet lamination process is illustrated in Figure 8 [92]. The top surface of a thin aluminum tape is contacted with the vibrating sonotrode. With the application of mechanical load, asperities are formed on the top surface of the tape, due to shear deformation and temperature increase. When the next layer of aluminum tape is applied, the compression and shear deformations cause the asperities to form a bonded interface. With the further addition of layers, the shear textures at the interface are formed. It is observed that the interface shows a equiaxed grain structure.

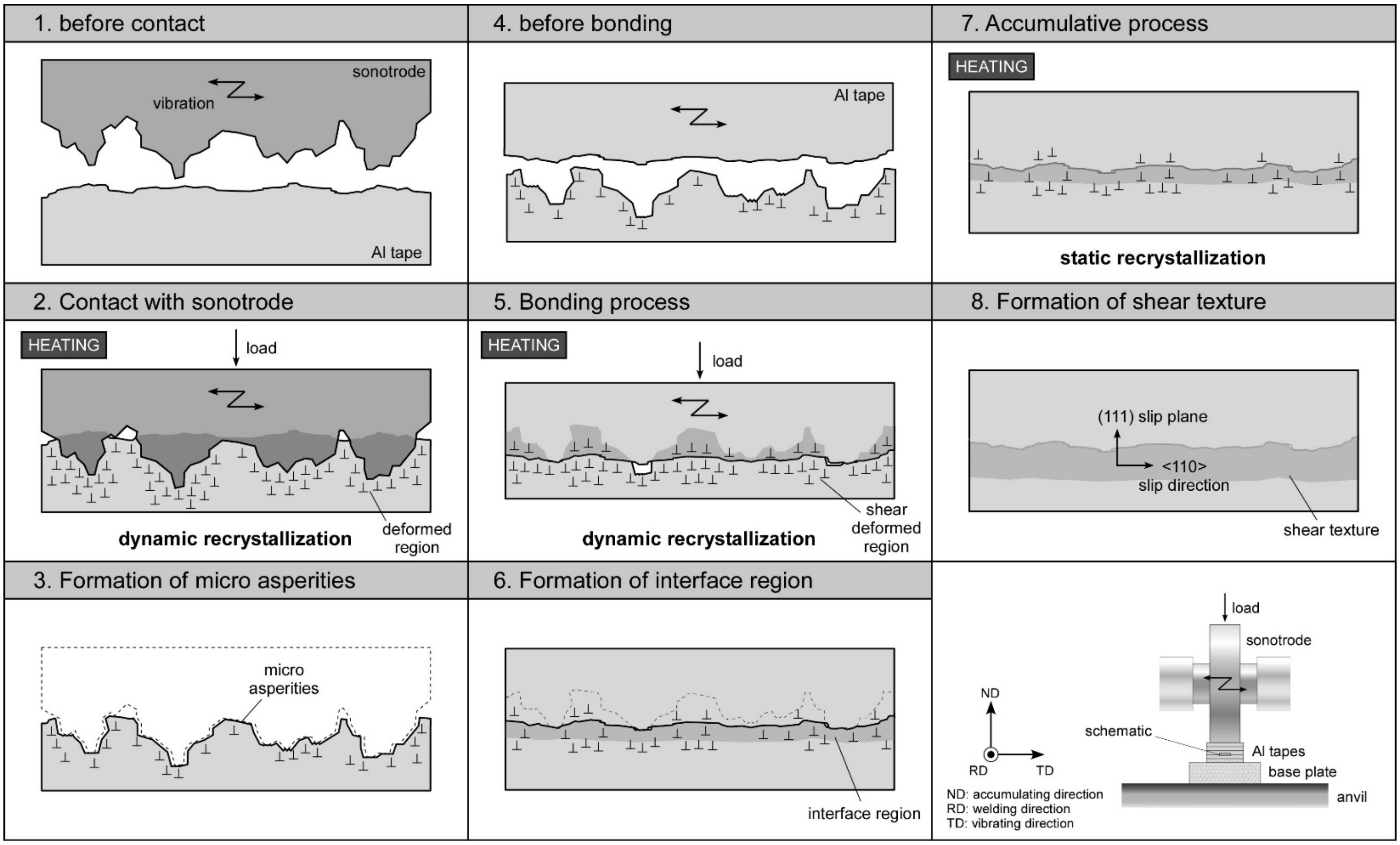

Figure 8: Microstructure evolutions during the UAM process[92].

In the sheet lamination process, temperature increases in the localized areas due to dynamic recrystallization associated with bonding. This heating process is mostly affected by vibration amplitude, where higher amplitude leads to higher dynamic plastic shear strain at the asperities. Aside from the processing parameters, metals with a higher strength show higher peak temperature than the low-strength ones [93].

The failure and fracture of the part in the accumulating direction are dominated by interface delamination. Aside from interface bonding strength, the layer thickness is also a major factor that influences the fracture resistance, due to thermal residual stress[94]. Even though sheet laminated products often show high hardness, good wear resistance, and high tensile compressive strength, the strength in the accumulating direction (Figure 7) is much weaker than the other two directions [95]. Sridharan *et al.* pointed out the anisotropic properties in fabricated Al6061. The accumulating direction always shows low mechanical properties, even with fully bonded interfaces without voids.

This is due to the migration of pre-existing shear bands and subsequently formed microvoids [96]. In Gussev *et al*. work, the Al6061 alloy was fabricated by the UAM process, and then subjected to tensile test [97]. As shown in Table 6, the parts in accumulating direction, or Z direction, fractured at only one fourth of its bulk's yield strength. By using material aging, the mechanical properties show a remarkable enhancement in the yield and ultimate strengths. Furthermore, Wolcott *et al.* optimized the UAM processing parameters, along with heat treatments, to enhance the Z direction properties [98] (Table 6). In their work, non-uniform metal layers were laminated using the tape to tape overlap technique. Optimal sonotrode surface roughness was achieved. Kunnek *et al.* studied the fatigue failure mechanisms of the alternating layered AA1050A/AA5005 composite [99]. They found that by mixing two different aluminum sheets alternatively, the cyclic stability and fatigue life were improved and better than those of pure aluminum alloy. With proper design, the anisotropy of sheet laminated metals can show some advantages. For example, in a study done by Kum *et al.* [100], the laminated carbon steel composite can resist higher impact energy in the normal direction to the sheet metal surface plane. This is due to the fact that delamination causes notch blunting or change of failure mode. Also, it was shown that in certain orientations of sheet laminated metals, the fatigue and crack rates were lower than those of the component materials. For composite materials, the tensile strength and ductility follow the mixing rule when the ductility of each material is similar. If the dissimilarity is large, then the mixing rule does not apply to the ductility of the composite[101].

Table 6: Mechanical properties of aluminum alloys fabricated by sheet lamination process

Process	Condition	Material	Orientation	Yield strength (MPa)	Ultimate strength (MPa)	Failure strain
Wrought [97]	As fabricated	Al6061	N/A	294	315	0.154
	Heat treated			277	311	0.188
UAM (Fabrisonic) [97]	As fabricated	Al6061	X	217	225	0.223
			Y	221	224	0.06
			Z	46*	--	--
	Heat treated		X	254	313	0.144
			Y	260	315	0.136
			Z	178*	--	--
Wrought [98]	As fabricated	Al3003	N/A	N/A	266	0.031
	Annealed			N/A	337	0.125
	Solutioned and aged			N/A	121	0.186
UAM (Fabrisonic SonicLayer 4000) [98]	As fabricated	Al3003	Z	N/A	136	0.014
	Annealed		Z	N/A	300	0.131
	Solutioned and aged		Z	N/A	117	0.137

* Fracture stress

The sheet lamination process can handle the fabrication of larger parts with faster production rates compared to other AM techniques. Additionally, the sheet lamination process often costs less, since it forms the part from metal sheets, which are less expensive than fine powders. Layered composite material with different metals could be fabricated by using sheet lamination process, which is a challenge for other AM techniques. Also, it provides better geometric accuracy in both rolling direction and vibrating direction, since the metal sheets are precisely cut. However, in the accumulating direction, the geometric dimension is hard to control, since the layer thickness changes during consolidation under pressure [102].

6. Conclusion and future research directions

In this review article, the latest AM techniques for metals are reviewed with the focus on the major AM processes, AM parts' microstructures and mechanical properties. Four commonly used AM techniques including powder bed fusion, direct energy deposition, metal binder jetting, and sheet lamination, are presented. For each individual technique, the AM materials are discussed in terms of their microstructure and mechanical properties.

Looking forward, there are several topics which require further investigation. The interrelations among AM processing parameters, part's microstructures, and mechanical properties are still not fully understood. To advance the understanding, theoretical studies using AM process modeling can be considered [48]. These theoretical process models could include heat and mass transfer, melting pool prediction, residual stress and distortion evolution, atomistic diffusion, densification, phase change etc. These models are crucial to fully understanding the structure-property relations. They can also be used to predict and optimize the target physical and mechanical properties, and develop strategies for AM materials design or inverse design.

Another potential research direction of AM systems is the production efficiency. There is always a balance between the production efficiency and product quality. Higher energy power or faster scanning speed will increase the production rate, but the product quality may be sacrificed since microstructures may vary. To address this issue, optimization of process parameters is required for the future design and application of AM techniques. On the other hand, complicated post-processing techniques also limit the production efficiency. Efficient methods for post processing, including removal of support material and heat treatment processes, need to be developed.

Finally, the AM fabricated material property database and the standards are still being established. It is still an ongoing effort to establish a comprehensive database to ensure the quality consistency of AM products.

Acknowledgements

JZ and YZ acknowledge the financial support provided by Walmart Foundation (project title: Optimal Plastic Injection Molding Tooling Design and Production through Advanced Additive Manufacturing). The authors are deeply indebted to the anonymous reviewers for their meticulous and constructive comments.

References

1. Wong, K.V. and A. Hernandez, *A review of additive manufacturing.* ISRN Mechanical Engineering, 2012. **2012**.
2. Ashley, S., *Rapid prototyping is coming of age.* Mechanical Engineering, 1995. **117**(7): p. 62.
3. Marks, P., *3D printing takes off with the world's first printed plane.* New Scientist, 2011. **211**(2823): p. 17-18.
4. Campbell, T., C. Williams, O. Ivanova, and B. Garrett, *Could 3D printing change the world.* Technologies, Potential, and Implications of Additive Manufacturing, Atlantic Council, Washington, DC, 2011.
5. Bak, D., *Rapid prototyping or rapid production? 3D printing processes move industry towards the latter.* Assembly Automation, 2003. **23**(4): p. 340-345.
6. Bartolotta, P.A., *Titanium Aluminide Applications in the High Speed Civil Transport*. 1999.
7. Wu, T., S.A. Jahan, P. Kumaar, A. Tovar, H. El-Mounayri, Y. Zhang, J. Zhang, D. Acheson, K. Brand, and R. Nalim, *A Framework for Optimizing the Design of Injection Molds with Conformal Cooling for Additive Manufacturing.* Procedia Manufacturing, 2015. **1**: p. 404-415.
8. F2792-12a, A.S.T.M., *Standard terminology for additive manufacturing technologies*, in *ASTM International*. 2015: West Conshohocken, PA.
9. International, A. *Committee F42 on Additive Manufacturing Technologies*. 2009 [cited 2017 03/08].
10. Ladd, C., J.H. So, J. Muth, and M.D. Dickey, *3D Printing of Free Standing Liquid Metal Microstructures.* Advanced Materials, 2013. **25**(36): p. 5081-5085.
11. Zenou, M., A. Sa’ar, and Z. Kotler, *Laser jetting of femto-liter metal droplets for high resolution 3D printed structures.* Scientific Reports, 2015. **5**: p. 17265.
12. Visser, C.W., R. Pohl, C. Sun, G.W. Roemer, B.H. in 't Veld, and D. Lohse, *Toward 3D Printing of Pure Metals by Laser-Induced Forward Transfer.* Advanced Materials, 2015. **27**(27): p. 4087-4092.
13. Lu, P.K., W. Li, and J.J. Lannutti, *Density gradients and the expansion-shrinkage transition during sintering.* Acta Materialia, 2004. **52**(7): p. 2057-66.
14. Procopio, A.T. and A. Zavaliangos, *Simulation of multi-axial compaction of granular media from loose to high relative densities.* Journal of the Mechanics and Physics of Solids, 2005. **53**(7): p. 1523-1551.
15. Antony, S.J., R.O. Momoh, and M.R. Kuh, *Micromechanical modelling of oval particulates subjected to bi-axial compression.* Computational Materials Science, 2004. **29**(4): p. 494-8.
16. Liu, L., *Simulation of microstructural evolution during isostatic compaction of monosized spheres.* Journal of Physics D (Applied Physics), 2003. **36**(15): p. 1881-9.
17. Yang, R.Y., R.P. Zou, and A.B. Yu, *Effect of material properties on the packing of fine particles.* Journal of Applied Physics, 2003. **94**(5): p. 3025-34.
18. Parhami, F. and R.M. McMeeking, *A network model for initial stage sintering.* Mechanics of Materials, 1998. **27**(2): p. 111-24.

19. Luding, S., R. Tykhoniak, and J. Tomas, *Anisotropic material behavior in dense, cohesive-frictional powders.* Chemical Engineering and Technology, 2003. **26**(12): p. 1229-1232.
20. Argento, C. and D. Bouvard, *Modeling the effective thermal conductivity of random packing of spheres through densification.* International Journal of Heat and Mass Transfer, 1996. **39**(7): p. 1343-1350.
21. Thornton, C., M.T. Ciomocos, and M.J. Adams, *Numerical simulations of diametrical compression tests on agglomerates.* Powder Technology, 2004. **140**(3): p. 258-267.
22. Groger, T., U. Tuzun, and D.M. Heyes, *Modelling and measuring of cohesion in wet granular materials.* Powder Technology, 2003. **133**(1-3): p. 203-215.
23. Zhou, Y.C., B.H. Xu, A.B. Yu, and P. Zulli, *An experimental and numerical study of the angle of repose of coarse spheres.* Powder Technology, 2002. **125**(1): p. 45-54.
24. D'Anna, G., *Mechanical properties of granular media, including snow, investigated by a low-frequency forced torsion pendulum.* Physical Review E (Statistical Physics, Plasmas, Fluids, and Related Interdisciplinary Topics), 2000. **62**(1): p. 982-92.
25. Wong, K.V. and A. Hernandez, *A Review of Additive Manufacturing.* ISRN Mechanical Engineering, 2012. **2012**: p. 10.
26. Murr, L.E., S.M. Gaytan, D.A. Ramirez, E. Martinez, J. Hernandez, K.N. Amato, P.W. Shindo, F.R. Medina, and R.B. Wicker, *Metal Fabrication by Additive Manufacturing Using Laser and Electron Beam Melting Technologies.* Journal of Materials Science & Technology, 2012. **28**(1): p. 1-14.
27. Tapia, G. and A. Elwany, *A Review on Process Monitoring and Control in Metal-Based Additive Manufacturing.* Journal of Manufacturing Science and Engineering, 2014. **136**(6): p. 060801-060801-10.
28. Frazier, W.E., *Metal Additive Manufacturing: A Review.* Journal of Materials Engineering and Performance, 2014. **23**(6): p. 1917-1928.
29. Sames, W.J., F.A. List, S. Pannala, R.R. Dehoff, and S.S. Babu, *The metallurgy and processing science of metal additive manufacturing.* International Materials Reviews, 2016. **61**(5): p. 315-360.
30. Olakanmi, E.O., R.F. Cochrane, and K.W. Dalgarno, *A review on selective laser sintering/melting (SLS/SLM) of aluminium alloy powders: Processing, microstructure, and properties.* Progress in Materials Science, 2015. **74**: p. 401-477.
31. Sing, S.L., J. An, W.Y. Yeong, and F.E. Wiria, *Laser and electron-beam powder-bed additive manufacturing of metallic implants: A review on processes, materials and designs.* Journal of Orthopaedic Research, 2016. **34**(3): p. 369-385.
32. Lewandowski, J.J. and M. Seifi, *Metal additive manufacturing: a review of mechanical properties.* Annual Review of Materials Research, 2016. **46**: p. 151-186.
33. Seifi, M., A. Salem, J. Beuth, O. Harrysson, and J.J. Lewandowski, *Overview of Materials Qualification Needs for Metal Additive Manufacturing.* JOM, 2016. **68**(3): p. 747-764.
34. Bourell, D.L., *Perspectives on Additive Manufacturing.* Annual Review of Materials Research, 2016. **46**: p. 1-18.
35. Kempen, K., L. Thijs, E. Yasa, M. Badrossamay, W. Verheecke, and J. Kruth. *Process optimization and microstructural analysis for selective laser melting of AlSi10Mg*. in *Solid Freeform Fabrication Symposium*. 2011.

36. Jamshidinia, M., F. Kong, and R. Kovacevic, *Numerical Modeling of Heat Distribution in the Electron Beam Melting® of Ti-6Al-4V.* Journal of Manufacturing Science and Engineering, 2013. **135**(6): p. 061010-061010.
37. Zhang, J., Y. Zhang, X. Guo, W.H. Lee, B. Hu, Z. Lu, Y.-G. Jung, and H. Lee, *Characterization of Microstructure and Mechanical Properties of Direct Metal Laser Sintered 15-5 Ph1 Stainless Steel Powders and Components*, in *TMS 2016: 145th Annual Meeting & Exhibition: Supplemental Proceedings*. 2016, John Wiley & Sons, Inc. p. 13-19.
38. Thijs, L., F. Verhaeghe, T. Craeghs, J.V. Humbeeck, and J.-P. Kruth, *A study of the microstructural evolution during selective laser melting of Ti–6Al–4V.* Acta Materialia, 2010. **58**(9): p. 3303-3312.
39. Zhai, Y., H. Galarraga, and D.A. Lados, *Microstructure, static properties, and fatigue crack growth mechanisms in Ti-6Al-4V fabricated by additive manufacturing: LENS and EBM.* Engineering Failure Analysis, 2016. **69**: p. 3-14.
40. Hunt, J.D., *Steady state columnar and equiaxed growth of dendrites and eutectic.* Materials Science and Engineering, 1984. **65**(1): p. 75-83.
41. Nastac, L., J. Valencia, M. Tims, and F. Dax, *Advances in the solidification of IN718 and RS5 Alloys.* Proceedings of Superalloys 718, 625, 706 and Various Derivatives, 2001.
42. Sames, W.J., K.A. Unocic, R.R. Dehoff, T. Lolla, and S.S. Babu, *Thermal effects on microstructural heterogeneity of Inconel 718 materials fabricated by electron beam melting.* Journal of Materials Research, 2014. **29**(17): p. 1920-1930.
43. Dehoff, R.R., M.M. Kirka, F.A. List, K.A. Unocic, and W.J. Sames, *Crystallographic texture engineering through novel melt strategies via electron beam melting: Inconel 718.* Materials Science and Technology, 2015. **31**(8): p. 939-944.
44. Helmer, H.E., C. Körner, and R.F. Singer, *Additive manufacturing of nickel-based superalloy Inconel 718 by selective electron beam melting: Processing window and microstructure.* Journal of Materials Research, 2014. **29**(17): p. 1987-1996.
45. Mazur, M., M. Leary, M. McMillan, S. Sun, D. Shidid, and M. Brandt, *5 - Mechanical properties of Ti6Al4V and AlSi12Mg lattice structures manufactured by Selective Laser Melting (SLM)*, in *Laser Additive Manufacturing*. 2017, Woodhead Publishing. p. 119-161.
46. Liu, Q., Y. Wang, H. Zheng, K. Tang, L. Ding, H. Li, and S. Gong, *Microstructure and mechanical properties of LMD–SLM hybrid forming Ti6Al4V alloy.* Materials Science and Engineering: A, 2016. **660**: p. 24-33.
47. Kunze, K., T. Etter, J. Grässlin, and V. Shklover, *Texture, anisotropy in microstructure and mechanical properties of IN738LC alloy processed by selective laser melting (SLM).* Materials Science and Engineering: A, 2015. **620**: p. 213-222.
48. Zhang, Y. and J. Zhang, *Sintering phenomena and mechanical strength of nickel based materials in direct metal laser sintering process—a molecular dynamics study.* Journal of Materials Research, 2016. **31**(15): p. 2233-2243.
49. Zhang, Y., L. Wu, H. El-Mounayri, K. Brand, and J. Zhang, *Molecular Dynamics Study of the Strength of Laser Sintered Iron Nanoparticles.* Procedia Manufacturing, 2015. **1**: p. 296-307.
50. Kruth, J.P., P. Mercelis, J. Van Vaerenbergh, L. Froyen, and M. Rombouts, *Binding mechanisms in selective laser sintering and selective laser melting.* Rapid Prototyping Journal, 2005. **11**(1): p. 26-36.

51. Yang, X. and C. Richard Liu, *Machining titanium and its alloys.* Machining Science and Technology, 1999. **3**(1): p. 107-139.
52. Mower, T.M. and M.J. Long, *Mechanical behavior of additive manufactured, powder-bed laser-fused materials.* Materials Science and Engineering: A, 2016. **651**: p. 198-213.
53. Qiu, C., N.J.E. Adkins, and M.M. Attallah, *Microstructure and tensile properties of selectively laser-melted and of HIPed laser-melted Ti–6Al–4V.* Materials Science and Engineering: A, 2013. **578**: p. 230-239.
54. Simonelli, M., Y.Y. Tse, and C. Tuck, *The formation of α + β microstructure in as-fabricated selective laser melting of Ti–6Al–4V.* Journal of Materials Research, 2014. **29**(17): p. 2028-2035.
55. Vilaro, T., C. Colin, and J.D. Bartout, *As-Fabricated and Heat-Treated Microstructures of the Ti-6Al-4V Alloy Processed by Selective Laser Melting.* Metallurgical and Materials Transactions A, 2011. **42**(10): p. 3190-3199.
56. Galarraga, H., D.A. Lados, R.R. Dehoff, M.M. Kirka, and P. Nandwana, *Effects of the microstructure and porosity on properties of Ti-6Al-4V ELI alloy fabricated by electron beam melting (EBM).* Additive Manufacturing, 2016. **10**: p. 47-57.
57. Hrabe, N. and T. Quinn, *Effects of processing on microstructure and mechanical properties of a titanium alloy (Ti–6Al–4V) fabricated using electron beam melting (EBM), Part 2: Energy input, orientation, and location.* Materials Science and Engineering: A, 2013. **573**: p. 271-277.
58. Rafi, H.K., N. Karthik, T.L. Starr, and B.E. Stucker. *Mechanical property evaluation of Ti-6Al-4V parts made using electron beam melting.* in *Proceedings of the Solid Freeform Fabrication Symposium*. 2012.
59. Facchini, L., E. Magalini, P. Robotti, and A. Molinari, *Microstructure and mechanical properties of Ti ‐ 6Al ‐ 4V produced by electron beam melting of pre ‐ alloyed powders.* Rapid Prototyping Journal, 2009. **15**(3): p. 171-178.
60. Krishnan, M., *Investigation of material and mechanical properties of Al alloy and Al based MMC parts produced by DMLS for industrial application*. 2014, Politecnico di Torino. p. 124.
61. Rafi, H.K., T.L. Starr, and B.E. Stucker, *A comparison of the tensile, fatigue, and fracture behavior of Ti–6Al–4V and 15-5 PH stainless steel parts made by selective laser melting.* The International Journal of Advanced Manufacturing Technology, 2013. **69**(5): p. 1299-1309.
62. Riemer, A., S. Leuders, M. Thöne, H.A. Richard, T. Tröster, and T. Niendorf, *On the fatigue crack growth behavior in 316L stainless steel manufactured by selective laser melting.* Engineering Fracture Mechanics, 2014. **120**: p. 15-25.
63. Mudge, R.P. and N.R. Wald, *Laser engineered net shaping advances additive manufacturing and repair.* WELDING JOURNAL-NEW YORK-, 2007. **86**(1): p. 44.
64. Domack, M.S., K.M. Taminger, and M. Begley. *Metallurgical Mechanisms Controlling Mechanical Properties of Aluminium Alloy 2219 Produced by Electron Beam Freeform Fabrication*. in *Materials science forum*. 2006. Trans Tech Publ.
65. Griffith, M., D. Keicher, and C. Atwood, *Free form fabrication of metallic components using laser engineered net shaping (LENS {trademark}).* 1996, Sandia National Labs., Albuquerque, NM (United States).

66. Griffith, M., D. Keicher, J. Romero, J. Smugeresky, C. Atwood, L. Harwell, and D. Greene. *Laser Engineered Net Shaping (LENS) for Fabrication of Metallic Components*. in *ASME International Mechanical Engineering Congress and Exposition*. 1996.
67. Wu, X., J. Liang, J. Mei, C. Mitchell, P.S. Goodwin, and W. Voice, *Microstructures of laser-deposited Ti–6Al–4V.* Materials & Design, 2004. **25**(2): p. 137-144.
68. Wang, F., J. Mei, and X. Wu, *Microstructure study of direct laser fabricated Ti alloys using powder and wire.* Applied Surface Science, 2006. **253**(3): p. 1424-1430.
69. Wu, X., R. Sharman, J. Mei, and W. Voice, *Microstructure and properties of a laser fabricated burn-resistant Ti alloy.* Materials & Design, 2004. **25**(2): p. 103-109.
70. Wang, T., Y.Y. Zhu, S.Q. Zhang, H.B. Tang, and H.M. Wang, *Grain morphology evolution behavior of titanium alloy components during laser melting deposition additive manufacturing.* Journal of Alloys and Compounds, 2015. **632**: p. 505-513.
71. Kobryn, P. and S. Semiatin. *Mechanical properties of laser-deposited Ti-6Al-4V*. in *Solid Freeform Fabrication Proceedings*. 2001. Austin.
72. Alcisto, J., A. Enriquez, H. Garcia, S. Hinkson, T. Steelman, E. Silverman, P. Valdovino, H. Gigerenzer, J. Foyos, J. Ogren, J. Dorey, K. Karg, T. McDonald, and O.S. Es-Said, *Tensile Properties and Microstructures of Laser-Formed Ti-6Al-4V.* Journal of Materials Engineering and Performance, 2011. **20**(2): p. 203-212.
73. Sterling, A.J., B. Torries, N. Shamsaei, S.M. Thompson, and D.W. Seely, *Fatigue behavior and failure mechanisms of direct laser deposited Ti–6Al–4V.* Materials Science and Engineering: A, 2016. **655**: p. 100-112.
74. Qiu, C., G.A. Ravi, C. Dance, A. Ranson, S. Dilworth, and M.M. Attallah, *Fabrication of large Ti–6Al–4V structures by direct laser deposition.* Journal of Alloys and Compounds, 2015. **629**: p. 351-361.
75. Ruff, P.E., *Effect of Manufacturing Processes on Structural Allowables Phase 2*. 1986, DTIC Document.
76. Tayon, W.A., R.N. Shenoy, M.R. Redding, R. Keith Bird, and R.A. Hafley, *Correlation Between Microstructure and Mechanical Properties in an Inconel 718 Deposit Produced Via Electron Beam Freeform Fabrication.* Journal of Manufacturing Science and Engineering, 2014. **136**(6): p. 061005-061005-7.
77. Sachs, E.M., J.S. Haggerty, M.J. Cima, and P.A. Williams, *Three-dimensional printing techniques*. 1993, Google Patents.
78. Sodhi, D.S., *Nonsimultaneous crushing during edge indentation of freshwater ice sheets.* Cold Regions Science and Technology, 1998. **27**(3): p. 179-195.
79. Turker, M., D. Godlinski, and F. Petzoldt, *Effect of production parameters on the properties of IN 718 superalloy by three-dimensional printing.* Materials Characterization, 2008. **59**(12): p. 1728-1735.
80. Mostafaei, A., Y. Behnamian, Y.L. Krimer, E.L. Stevens, J.L. Luo, and M. Chmielus, *Effect of solutionizing and aging on the microstructure and mechanical properties of powder bed binder jet printed nickel-based superalloy 625.* Materials & Design, 2016. **111**: p. 482-491.
81. Mostafaei, A., J. Toman, E.L. Stevens, E.T. Hughes, Y.L. Krimer, and M. Chmielus, *Microstructural evolution and mechanical properties of differently heat-treated binder jet printed samples from gas- and water-atomized alloy 625 powders.* Acta Materialia, 2017. **124**: p. 280-289.

82. Dilip, J.J.S., H. Miyanaji, A. Lassell, T.L. Starr, and B. Stucker, *A novel method to fabricate TiAl intermetallic alloy 3D parts using additive manufacturing.* Defence Technology.
83. Mostafaei, A., E.L. Stevens, E.T. Hughes, S.D. Biery, C. Hilla, and M. Chmielus, *Powder bed binder jet printed alloy 625: Densification, microstructure and mechanical properties.* Materials & Design, 2016. **108**: p. 126-135.
84. Hong, D., D.T. Chou, O.I. Velikokhatnyi, A. Roy, B. Lee, I. Swink, I. Issaev, H.A. Kuhn, and P.N. Kumta, *Binder-jetting 3D printing and alloy development of new biodegradable Fe-Mn-Ca/Mg alloys.* Acta Biomater, 2016. **45**: p. 375-386.
85. Bai, Y. and C.B. Williams, *An exploration of binder jetting of copper.* Rapid Prototyping Journal, 2015. **21**(2): p. 177-185.
86. Meaney, R., I.J. Jordaan, and J. Xiao, *Analysis of medium scale ice-indentation tests.* Cold Regions Science and Technology, 1996. **24**(3): p. 279-287.
87. Zhang, Y., L. Wu, X. Guo, Y.-G. Jung, and J. Zhang, *Molecular dynamics simulation of electrical resistivity in sintering process of nanoparticle silver inks.* Computational Materials Science, 2016. **125**: p. 105-109.
88. Obikawa, T., M. Yoshino, and J. Shinozuka, *Sheet steel lamination for rapid manufacturing.* Journal of Materials Processing Technology, 1999. **89–90**: p. 171-176.
89. White, D., *Ultrasonic object consolidation*. 2003, Google Patents.
90. White, D.R., *Ultrasonic consolidation of aluminum tooling.* Advanced materials & processes, 2003. **161**(1): p. 64-65.
91. Dehoff, R.R. and S.S. Babu, *Characterization of interfacial microstructures in 3003 aluminum alloy blocks fabricated by ultrasonic additive manufacturing.* Acta Materialia, 2010. **58**(13): p. 4305-4315.
92. Fujii, H.T., M.R. Sriraman, and S.S. Babu, *Quantitative Evaluation of Bulk and Interface Microstructures in Al-3003 Alloy Builds Made by Very High Power Ultrasonic Additive Manufacturing.* Metallurgical and Materials Transactions A, 2011. **42**(13): p. 4045-4055.
93. Sriraman, M.R., M. Gonser, H.T. Fujii, S.S. Babu, and M. Bloss, *Thermal transients during processing of materials by very high power ultrasonic additive manufacturing.* Journal of Materials Processing Technology, 2011. **211**(10): p. 1650-1657.
94. John J. Lewandowski and W.H. Hunt, *Intrinsic and Extrinsic Fracture Mechanisms in Inorganic Composite Systems* 1995: The Minerals, Metals & Materials Society.
95. Shimizu, S., H.T. Fujii, Y.S. Sato, H. Kokawa, M.R. Sriraman, and S.S. Babu, *Mechanism of weld formation during very-high-power ultrasonic additive manufacturing of Al alloy 6061.* Acta Materialia, 2014. **74**: p. 234-243.
96. Sridharan, N., M. Gussev, R. Seibert, C. Parish, M. Norfolk, K. Terrani, and S.S. Babu, *Rationalization of anisotropic mechanical properties of Al-6061 fabricated using ultrasonic additive manufacturing.* Acta Materialia, 2016. **117**: p. 228-237.
97. Gussev, M.N., N. Sridharan, M. Norfolk, K.A. Terrani, and S.S. Babu, *Effect of post weld heat treatment on the 6061 aluminum alloy produced by ultrasonic additive manufacturing.* Materials Science and Engineering: A, 2017. **684**: p. 606-616.
98. Wolcott, P.J., A. Hehr, C. Pawlowski, and M.J. Dapino, *Process improvements and characterization of ultrasonic additive manufactured structures.* Journal of Materials Processing Technology, 2016. **233**: p. 44-52.

99. Kümmel, F., T. Hausöl, H.W. Höppel, and M. Göken, *Enhanced fatigue lives in AA1050A/AA5005 laminated metal composites produced by accumulative roll bonding.* Acta Materialia, 2016. **120**: p. 150-158.
100. Kum, D.W., T. Oyama, J. Wadsworth, and O.D. Sherby, *The impact properties of laminated composites containing ultrahigh carbon (UHC) steels.* Journal of the Mechanics and Physics of Solids, 1983. **31**(2): p. 173-186.
101. Lee, S., J. Wadsworth, and O.D. Sherby, *Tensile Properties of Laminated Composites Based on Ultrahigh Carbon Steel.* Journal of Composite Materials, 1991. **25**(7): p. 842-853.
102. Mueller, B. and D. Kochan, *Laminated object manufacturing for rapid tooling and patternmaking in foundry industry.* Computers in Industry, 1999. **39**(1): p. 47-53.

List of figures

List of tables